Pediatr Transplantation 2013: 17: E29–E32

Pediatric Transplantation
DOI: 10.1111/j.1399-3046.2012.01762.x

Successful bone marrow transplantation with reduced intensity conditioning in a patient with delayed-onset adenosine deaminase deficiency

Kanegane H, Taneichi H, Nomura K, Wada T, Yachie A, Imai K, Ariga T, Santisteban I, Hershfield MS, Miyawaki T. Successful bone marrow transplantation with reduced intensity conditioning in a patient with delayed-onset adenosine deaminase deficiency.

Abstract: In this case report, we describe successful BMT with RIC in a patient with delayed-onset ADA deficiency. A three-yr-old Japanese boy was diagnosed with delayed-onset ADA deficiency because of recurrent bronchitis, bronchiectasia, and lymphopenia. In addition, autoimmune thyroiditis and neutropenia were present. At four yr of age, he underwent BMT with a RIC regimen, including busulfan and fludarabine, from an HLA-identical healthy sister. Engraftment after BMT was uneventful without GVHD. Decreased ADA levels in blood immediately increased following BMT, and the patient was disease-free 13 months after BMT. These results suggest that BMT with RIC may sufficiently restore immune regulation in delayed-onset ADA deficiency. A longer follow-up period is needed to confirm these observations.

Hirokazu Kanegane[1], Hiromichi Taneichi[1], Keiko Nomura[1], Taizo Wada[2], Akihiro Yachie[2], Kohsuke Imai[3], Tadashi Ariga[4], Ines Santisteban[5], Michael S. Hershfield[5] and Toshio Miyawaki[1]

[1]Department of Pediatrics, Graduate School of Medicine and Pharmaceutical Sciences, University of Toyama, Toyama, Japan, [2]Department of Pediatrics, School of Medicine, Institute of Medical, Pharmaceutical and Health Sciences, Kanazawa University, Kanazawa, Japan, [3]Department of Community Pediatrics, Perinatal and Maternal Medicine, Graduate School of Medicine, Tokyo Medical and Dental University, Tokyo, Japan, [4]Department of Pediatrics, Hokkaido University Graduate School of Medicine, Sapporo, Japan, [5]Department of Medicine and Biochemistry, Duke University Medical Center, Durham, NC, USA

Key words: adenosine deaminase deficiency – delayed-onset – bone marrow transplantation – reduced intensity conditioning

Hirokazu Kanegane, Department of Pediatrics, Graduate School of Medicine and Pharmaceutical Sciences, University of Toyama, 2630 Sugitani, Toyama, Toyama 930-0194, Japan
Tel.: 81 76 434 7313
Fax: 81 76 434 5029
E-mail: kanegane@med.u-toyama.ac.jp

Accepted for publication 29 May 2012

ADA deficiency is a disorder of purine metabolism, which results in abnormalities in immune system development and function (1, 2). A majority of ADA deficiency cases indicate SCID during infancy; however, approximately 15% of ADA-deficient patients present with symptoms after infancy, which is referred to as a delayed- or late-onset type. Patients with delayed-onset ADA deficiency exhibit variable clinical symptoms, including bacterial infections and autoimmune manifestations. Allogeneic hematopoietic stem cell transplantation has long been a gold standard for the treatment of ADA-SCID; however, two other second-line options are available for ADA-SCID: Enzyme replacement therapy with PEG-ADA and hematopoietic stem cell gene therapy (3). The treatment of choice for delayed-onset ADA deficiency remains unclear because of

Abbreviation: ADA, adenosine deaminase; BMT, bone marrow transplantation; dAXP, deoxyadenosine nucleotides; GVHD, graft-versus-host disease; HLA, human leukocyte antigen; PEG, polyethylene-glycosylated; PEG-ADA, polyethylene-glycosylated bovine ADA; RIC, reduced intensity conditioning; SCID, severe combined immunodeficiency; sjKRECs, signal joint κ-deleting recombination excision circles; TCR, T-cell receptor; TRECs, T-cell receptor excision circles.

the clinical variety. We report on a four-yr-old Japanese boy with delayed-onset ADA deficiency who underwent BMT with RIC from a HLA-identical healthy sister.

Case report

The patient was previously described (4). He is a boy who was admitted to our hospital at three yr of age for the investigation of recurrent infectious episodes. The patient did not have a neurological deficit. Laboratory data revealed neutropenia (600/μL), lymphocytopenia (580/μL), elevated C-reactive protein (7.43 mg/dL; normal, <0.29 mg/dL) and elevated thyroid-stimulating hormone (133 μIU/mL; normal, 0.35–3.73 μIU/mL). Anti-neutrophil, anti-nuclear, anti-thyroglobulin, and anti-thyroid peroxidase antibodies were positive, indicating that autoimmune neutropenia and thyroiditis were present. Chest computed tomography disclosed bronchiectasia. An immunological study indicated hypergammaglobulinemia, but a low percentage of IgG2 subclass antibodies (5.41%; normal, 20–30%) was obtained. The lymphocyte subsets revealed an expansion of the $CD45RO^+$ (memory) populations of $CD4^+$ and $CD8^+$ T cells (74.8% and 39.6%, respectively) and an extremely reduced number of $CD20^+$ B cells (0.2%). TRECs and signal joint κ-deleting recombination excision circles (sjKRECs) were quantified by real-time PCR as previously described (5, 6) and were undetectable. Flow cytometry analysis of the TCR Vβ repertoire was performed as described previously (7), and the analysis revealed an extremely skewed pattern in $CD8^+$ T cells but not in $CD4^+$ T cells (Fig. 1). Therefore, the patient was clinically presumed to have a combined immunodeficiency with autoimmune manifestations, possibly indicating delayed-onset ADA deficiency. The ADA and dAXP levels in whole blood were measured using the extracts of dried blood spots (8). ADA was found to be decreased (1.0 μmol/h/mg protein; normal, 26.4 $\pm$ 10.0 μmol/h/mg protein), and %dAXP increased to 10.8% (normal $<$ 1%). These data led to a diagnosis of ADA deficiency. An analysis of the *ADA* gene disclosed that the patient had compound heterozygous mutations (R156C and V177M). This genotype is compatible with delayed-onset ADA deficiency (9, 10).

The patient was treated with intravenous immunoglobulin replacement therapy, and oral administration of trimethoprim–sulfamethoxazole, acyclovir, and levothyroxine. He was nearly free from infections; however, his serum immunoglobulin levels gradually decreased. We identified his healthy sister as an HLA-identical donor with no mutation in the *ADA* gene. At the age of four yr, the patient underwent BMT. He was treated with conditioning, which consisted of fludarabine (30 mg/m^2/day $\times$ six days, days -7 to -2) and intravenous reduced dose busulfan (4.4 mg/kg/day $\times$ two days, days -3 to -2). The patient received 6.9×10^8 nucleated cells/kg containing 3.1×10^6 $CD34^+$ cells/kg to achieve rapid engraftment. Cyclosporin A was used as GVHD prophylaxis. The post-transplant clinical course was without major complications, and no signs of acute GVHD were observed. The patient did not receive blood transfusion, and engraftments of neutrophils (>500/μL) and thrombocytes ($>50\,000$/μL) were achieved at days 18 and 35, respectively. Cyclosporin A was stopped at day 46. The patient is currently well and has not suffered from any major infectious episodes. The patient received levothyroxine at a low dose; however, anti-thyroglobulin and anti-thyroid peroxidase antibodies became negative. The patient went off immunoglobulin replacement therapy 11 months after BMT.

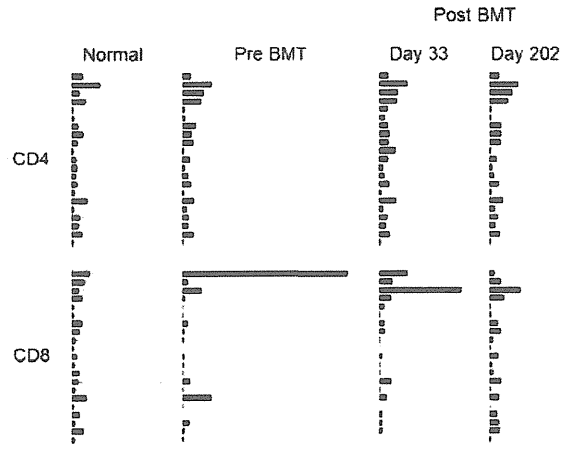

Fig. 1. TCR Vβ repertoire in the $CD4^+$ and $CD8^+$ T cells that were analyzed pre-BMT and post-BMT on days 23 and 202. The TCR Vβ repertoire was analyzed by flow cytometry as previously described (7).

Donor engraftment was evaluated by PCR amplification of the microsatellite marker D8S1179. Donor engraftment in granulocytes and B cells was observed at days 33 and 83, respectively. Complete donor engraftment in whole cells was achieved at day 323 (Table 1). Consistent with high chimerism, the patient exhibited a rapid increase in ADA activity and fast metabolic detoxification by day 83 (Table 2). In addition, immunological studies indicated rapid reconstitution of the lymphocyte subpopulation, and B cells increased to a normal level (305/μL;

Table 1. Engraftment of donor cells in different cell lineages

	Donor cell engraftment (%)				
Post-BMT	Whole blood	Lymphocytes	T cells	B cells	Granulocytes
Day 12	8.5	NA	14.2	NA	0
Day 33	50.7	33.0	NA	NA	100.0
Day 83	80.5	NA	16.5	100.0	100.0
Day 323	>95.0	NA	>95.0	100.0	100.0

NA, not applicable.
Analyses of donor cell engraftment according to a chimerism assay in the peripheral blood of the patient at different time points after BMT.

Table 2. ADA activity in the whole blood of the patient

Samples	ADA (μmol/h/mg protein)	%dAXP
Pre-BMT	1.0	10.8
Day 25	8.7	1.1
Day 83	33.7	0.0
ADA-SCID	0.38 ± 0.5	50.3 ± 18.0
Normal levels	26.4 ± 10.0	<1

The data are from the analyses of the extracts of dried blood spots.

age-matched control, 278–922/μL) at day 97 (Fig. 2). TREC and sjKREC levels reached normal levels at days 83 and 202, respectively (Table 3). The CD45RO$^+$ (memory) populations of CD4$^+$ T cells decreased to a normal range (21.9 ± 4.4%) soon after BMT. Sequential TCR Vβ repertoire analyses revealed that the polyclonal patterns in CD4$^+$ T cells were consistent after BMT, and the extremely skewed pattern in CD8$^+$ T cells had improved by day 202 (Fig. 1).

Discussion

ADA-SCID is a complex immune and metabolic disorder that results from a lack of ADA, which is a key enzyme in purine metabolism. Patients with ADA-SCID have recurrent and severe infections, growth retardation and organ failure. The first treatment of choice is BMT from an HLA-identical sibling donor, if available, followed by treatments for other forms of SCID. Second-line treatments for patients without an HLA-identical donor include enzyme replacement therapy with PEG-ADA, matched unrelated donor hematopoietic stem cell transplantation and hematopoietic stem cell gene therapy (3). Although the treatment strategy for ADA-SCID is well-established, treatment for delayed-onset ADA deficiency is not standardized because of the various clinical conditions. In this study, an HLA-identical healthy sibling donor was available, and we selected BMT from this donor to treat the patient. In cases of ADA-SCID, BMT from an HLA-identical donor is undertaken without a preparative conditioning regimen. The largest series of SCID patients from the European SCETIDE database included 475 patients (11). Of these patients, 51 patients with ADA-SCID had a three-yr survival rate of 81% for HLA-matched transplantation, but 29% for HLA-mismatched transplantation. A recently published cohort study demonstrated that hematopoietic stem cell transplantation in patients with SCID, including ADA deficiency, resulted in engraftment and long-term survival for the majority of patients with or without conditioning (12). However, transplantation without conditioning may result in partial donor engraftment, causing reduced immune reconstitution. Alternatively, hematopoietic stem cell gene therapy is effective for ADA-SCID patients who lack an HLA-identical sibling donor (13). Autologous CD34$^+$ bone marrow cells were transduced with a retroviral vector containing the ADA gene and infused into 10 patients with ADA-SCID after non-myeloablative conditioning. However, two patients have required enzyme replacement after gene therapy (14). ADA gene therapy has been performed in total 31 patients in Italy, the United Kingdom, and the United States. Twenty-one patients have been successful, whereas 10 patients have received enzyme replacement therapy (15). Recently, Cancrini et al. (16) described two ADA-SCID patients from the same family who both underwent BMT. One patient underwent BMT without conditioning, whereas

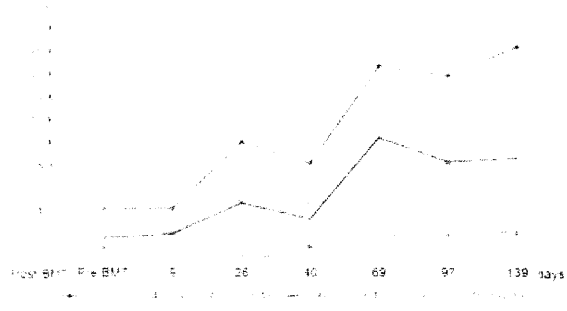

Fig. 2. Kinetics of the lymphocyte subpopulations in the patient.

Table 3. TREC and sjKREC levels as measured by quantitative PCR in the peripheral blood at different time points

	Post-BMT Day 25	Day 83	Day 202	Normal values
TRECs	0	8.1×10^3	1.9×10^3	$3.5 \pm 2.8 \times 10^3$
sjKRECs	0	2.8×10^2	6.4×10^3	$4.8 \pm 0.6 \times 10^3$
RNaseP	4.5×10^4	1.6×10^5	2.0×10^5	

All of the units are copies/μg DNA. The RNaseP gene was amplified as an internal control. The normal values indicate the copy numbers of the age-matched controls (2–6 yr of age).

the other patient was administered a RIC regimen (busulfan and fludarabine) following the failure of cord blood transplantation. Engraftment and immune reconstitution were compared in these patients. The patient who received conditioning exhibited stable mixed chimerism in all of the cell lineages, whereas the patient who underwent BMT without conditioning exhibited slow immune reconstitution, especially in B and myeloid cells. This observation indicated that the use of conditioning resulted in faster immunologic and metabolic reconstitution. In these patients, the immune reconstitution of B and myeloid cells was slower than that of T and NK cells. Interestingly, the reconstitution of myeloid and B cells appeared earlier than that of T cells in our patient. The patient with delayed-onset ADA deficiency had a substantial number of T cells but no B cells before BMT, and the generation of new T cells may take longer than B cells.

Patients with delayed-onset ADA deficiency often have chronic pulmonary insufficiency and autoimmune phenomena, including cytopenia and anti-thyroid antibodies, as observed in our patient. Patients with a delayed- or late-onset type may survive undiagnosed in the first decade of life or beyond; however, the longer the disease goes undiagnosed, the more the immune function deteriorates. The serum immunoglobulin levels of our patient gradually decreased from the point of diagnosis. Our patient had a substantial number of T cells; however, TRECs were undetectable in his peripheral blood. Therefore, we decided that the patient would receive BMT preceded by a RIC regimen, including busulfan and fludarabine. The use of RIC in BMT from an HLA-identical donor in this patient resulted in rapid and complete immune and metabolic reconstitution, and there was no treatment-related toxicity. However, a longer follow-up period is required to confirm these observations. If patients have an HLA-identical sibling donor, BMT with a RIC regimen may be the treatment of choice in patients with delayed-onset ADA deficiency.

Acknowledgments

We would like to thank Mr. Hitoshi Moriuchi, Ms. Chikako Sakai, and Ms. Junko Michino for their technical assistance, and Dr. Bobby Gaspar for critical discussions. We are also grateful to Drs. Hideyuki Nakaoka, Takuya Wada, Akiko Sugiyama, Xi Yang, Shunichiro Takezaki, Masafumi Yamada, Osamu Ohara, Shigeaki Nonoyama, and Chikako Kamae for their clinical and experimental support.

Source of funding

This work was supported by a Grant-in-Aid for Scientific Research from the Ministry of Education, Culture, Sports, Science and Technology of Japan and a grant for Research on Intractable Disease from the Ministry of Health, Labor and Welfare of Japan.

References

1. Hershfield MS. Combined immune deficiency due to purine enzyme defects. In: Stiehm ER, Ochs HD, Winkelstein JA, eds. Immunologic Disorders in Infants and Children. Philadelphia, PA: WB Saunders, 2004: pp. 480–504.
2. Hirshhorn R, Candotti F. Immunodeficiency disease due to defects of purine metabolism. In: Ochs HD, Smith CIE, Puck JM, eds. Primary Immunodeficiency Diseases: A Molecular and Genetic Approach. New York, NY: Oxford University Press, 2007: pp. 169–196.
3. Gaspar HB, Aiuti A, Porta F, Candotti F, Hershfield MS, Notarangelo LD. How I treat ADA deficiency. Blood 2009: 114: 3524–3532.
4. Nakaoka H, Kanegane H, Taneichi H, et al. Delayed onset adenosine deaminase deficiency associated with acute disseminated encephalomyelitis. Int J Hematol 2012: 95: 692–696.
5. Morinishi Y, Imai K, Nakagawa N, et al. Identification of severe combined immunodeficiency by T-cell receptor excision circles quantification using neonatal Guthrie cards. J Pediatr 2009: 155: 829–833.
6. Nakagawa N, Imai K, Kanegane H, et al. Quantification of κ-deleting recombination excision circles in Guthrie cards for the identification of early B-cell maturation defects. J Allergy Clin Immunol 2011: 128: 223–225.e2.
7. Toga A, Wada T, Sakakibara Y, et al. Clinical significance of cloned expansion and CD5 down-regulation in Epstein–Barr virus (EBV)-infected CD8+ T lymphocytes in EBV-associated hemophagocytic lymphohistiocytosis. J Infect Dis 2010: 201: 1923–1932.
8. Arrendondo-Vega FX, Santisteban I, Richard E, et al. Adenosine deaminase deficiency with mosaicism for a "second-site suppressor" of a splicing mutation: Decline in revertant T lymphocytes during enzyme replacement therapy. Blood 2002: 99: 1005–1013.
9. Arrendondo-Vega FX, Santisteban I, Daniels S, Toutain S, Hershfield MS. Adenosine deaminase deficiency: Genotype-phenotype correlations based expressed activity of 29 mutant alleles. Am J Hum Genet 1998: 63: 1049–1059.
10. Hershfield MS. Genotype is an important determinant of phenotype in adenosine deaminase deficiency. Curr Opin Immunol 2003: 15: 571–577.
11. Antoine C, Muller S, Cant A, et al. Long-term survival and transplantation of haematopoietic stem cells for immunodeficiencies: Report of the European experience 1968–99. Lancet 2003: 361: 553–560.
12. Patel NC, Chinen J, Rosenblatt HM, et al. Outcomes of patients with severe combined immunodeficiency treated with hematopoietic stem cell transplantation with and without preconditioning. J Allergy Clin Immunol 2009: 124: 1062–1069.
13. Aiuti A, Cattaneo F, Galimberti S, et al. Gene therapy for immunodeficiency due to adenosine deaminase deficiency. N Engl J Med 2009: 360: 447–458.
14. Aiuti A, Roncarrolo MG. Ten years of gene therapy for primary immunodeficiencies. Hematology Am Soc Hematol Educ Program 2009: 682–689.
15. Fischer A, Hacein-Bey-Abina S, Cavazzana-Calvo M. Gene therapy for primary adaptive immune deficiencies. J Allergy Clin Immunol 2011: 127: 1356–1359.
16. Cancrini C, Ferrua F, Scarselli A, et al. Role of reduced intensity conditioning in T-cell and B-cell immune reconstitution after HLA-identical bone marrow transplantation in ADA-SCID. Haematologica 2010: 95: 1778–1782.

OPEN ACCESS Freely available online

PLOS | ONE

DNA Methylation Profile Distinguishes Clear Cell Sarcoma of the Kidney from Other Pediatric Renal Tumors

Hitomi Ueno[1], Hajime Okita[1]*, Shingo Akimoto[1], Kenichiro Kobayashi[1], Kazuhiko Nakabayashi[2], Kenichiro Hata[2], Junichiro Fujimoto[3], Jun-ichi Hata[4], Masahiro Fukuzawa[5], Nobutaka Kiyokawa[1]

1 Department of Pediatric Hematology and Oncology Research, National Research Institute for Child Health and Development, Setagaya-ku, Tokyo, Japan, 2 Department of Maternal-Fetal Biology, National Research Institute for Child Health and Development, Setagaya-ku, Tokyo, Japan, 3 Director of Clinical Research Center, National Center for Child Health and Development, Setagaya-ku, Tokyo, Japan, 4 College of Human Science, Tokiwa University, Mito, Ibaraki, Japan, 5 President of Osaka Medical Center and Research Institute for Maternal and Child Health, Osaka Medical Center and Research Institute for Maternal and Child Health, Izumi, Osaka, Japan

Abstract

A number of specific, distinct neoplastic entities occur in the pediatric kidney, including Wilms' tumor, clear cell sarcoma of the kidney (CCSK), congenital mesoblastic nephroma (CMN), rhabdoid tumor of the kidney (RTK), and the Ewing's sarcoma family of tumors (ESFT). By employing DNA methylation profiling using Illumina Infinium HumanMethylation27, we analyzed the epigenetic characteristics of the sarcomas including CCSK, RTK, and ESFT in comparison with those of the non-neoplastic kidney (NK), and these tumors exhibited distinct DNA methylation profiles in a tumor-type-specific manner. CCSK is the most frequently hypermethylated, but least frequently hypomethylated, at CpG sites among these sarcomas, and exhibited 490 hypermethylated and 46 hypomethylated CpG sites in compared with NK. We further validated the results by MassARRAY, and revealed that a combination of four genes was sufficient for the DNA methylation profile-based differentiation of these tumors by clustering analysis. Furthermore, *THBS1* CpG sites were found to be specifically hypermethylated in CCSK and, thus, the DNA methylation status of these *THBS1* sites alone was sufficient for the distinction of CCSK from other pediatric renal tumors, including Wilms' tumor and CMN. Moreover, combined bisulfite restriction analysis could be applied for the detection of hypermethylation of a *THBS1* CpG site. Besides the biological significance in the pathogenesis, the DNA methylation profile should be useful for the differential diagnosis of pediatric renal tumors.

Citation: Ueno H, Okita H, Akimoto S, Kobayashi K, Nakabayashi K, et al. (2013) DNA Methylation Profile Distinguishes Clear Cell Sarcoma of the Kidney from Other Pediatric Renal Tumors. PLoS ONE 8(4): e62233. doi:10.1371/journal.pone.0062233

Editor: Qian Tao, The Chinese University of Hong Kong, Hong Kong

Received December 25, 2012; **Accepted** March 19, 2013; **Published** April 26, 2013

Funding: This work was supported by Health and Labour Sciences Research Grants (the 3rd-term comprehensive 10-year strategy for cancer control H22-011), Grant-in-Aid for Scientific Research (B)(23390405, Grant of National Center for Child Health and Development (22A-5, 24-4), and Program for Promotion of Fundamental Studies in Health Sciences of the National Institute of Biomedical Innovation (NIBIO, 10-41, -42, -43, -44, -45). The funders had no role in the study design, data collection and analysis, decision to publish, or preparation of the manuscript.

Competing Interests: The authors have declared that no competing interests exist.

* E-mail: okita-h@ncchd.go.jp

Introduction

In the pediatric population, the types of renal tumor are entirely different from those occurring in adults. It is estimated that 85% of pediatric renal malignancies comprise nephroblastoma, 5% congenital mesoblastic nephroma (CMN), 4% clear cell sarcoma of the kidney (CCSK), and 2% rhabdoid tumor of the kidney (RTK) [1], and these 4 major entities account for 96% of the total. The remaining 4% tend to occur in older children and include miscellaneous tumors, such as the Ewing's sarcoma family of tumors (ESFT). Nephroblastoma is malignant but still a relatively favorable tumor prognostically, being derived from nephrogenic blastemal cells that can show divergent differentiation. CMN is a kind of fibroblastic sarcoma of infancy and characterized by a specific chromosomal translocation, t(12;15)(p13;q25), which results in the fusion of *ETV6* and *NTRK3* genes [2]. On the other hand, CCSK is a relatively unfavorable tumor prognostically, being composed of clear mesenchymal cells with a characteristic vascular pattern [3]. RTK is a highly aggressive tumor occurring in young children, has a dismal outcome, and is characterized by pathological rhabdoid features and molecular biallelic inactivation of the *SMARCB1* (*hSNF5/INI1*) gene [4–6].

Since pediatric renal tumors are diverse neoplastic entities, as described above, and require different therapeutic strategies, rapid and accurate diagnosis is crucial for adequate treatment. However, all those tumors are composed of small-to-medium-sized, round, oval, or spindle-shaped undifferentiated or immature cells, and often deceptively mimic each other, making the diagnosis difficult [7]. In RTK and CMN, molecular markers, i.e., loss of SMARCB1 expression and *ETV6-NTRK3* fusion, respectively, are useful for an ancillary diagnosis, whereas the diagnosis of nephroblastoma and CCSK is exclusively based on histologic features. Although numerous studies have been done, immunohistochemical features or recurrent genetic changes that can reliably distinguish CCSKs from other pediatric renal tumors have not identified [3,8]. Therefore, the identification of molecular signatures that can distinguish CCSK from other renal tumors should be useful and provide diagnostic confidence and accuracy.

Alterations of DNA methylation have been well documented as an important peculiarity of cancer cells [9,10], and two patterns of

DNA-methylation changes have been observed in cancer [11,12]. One is a global hypomethylation associated with increased chromosomal instability, the reactivation of transposable elements, and loss of imprinting. The other is hypermethylation of CpG islands located in promoter regions of tumor suppressor genes that has conventionally been associated with transcriptional silencing in cancer. These aberrant DNA methylations are thought to be closely related to the development of cancer. Therefore, the identification of specific DNA methylation markers would be helpful for understanding the pathogenetic mechanism as well as for developing new therapeutic strategies. In Wilms' tumor, hypermethylation of *HACE1*, *RASSF1A* and *SIM1* and hypomethylation of *GRIPR* were reported [13–16], whereas the DNA methylation analysis in pediatric renal sarcomas including RTK, CCSK has not been reported yet.

In an attempt to investigate the characteristics of DNA methylation of pediatric sarcomas including CCSK, RTK, and ESFT, we performed DNA methylation analysis using Illumina Infinium HumanMethylation27. In this paper, we demonstrated that each sarcoma had a distinct DNA methylation profile and could be classified by the methylation pattern of a set of specific genes. We further proposed a convenient assay for the differential diagnosis of CCSK from other pediatric renal tumor.

Materials and Methods

Ethics Statement

This study was approved by the ethics committee/IRB at the National Center for Child Health and Development, and written informed consent was obtained from parents for samples from JWiTS. Since written informed consent was not obtained in a subset of samples collected before 2001, the identifying information for them was removed before analysis, in accordance with the Ethical Guideline for Clinical Research enacted by the Japanese Government. The ethics committee/IRB approved the waiver of written informed consent for latter samples.

Table 2. The number of hyper- and hypomethylated genes in comparison with non-neoplastic kidney.

	CpG island probe	
	Hypermethylated	**Hypomethylated**
CCSK	490 probes (437 genes)	46 probes (36 genes)
RTK	130 probes (107 genes)	65 probes (62 genes)
ESFT	66 probes (58 genes)	55 probes (46 genes)
	Non-CpG island probe	
	Hypermethylated	**Hypomethylated**
CCSK	184 probes (166 genes)	117probes (112 genes)
RTK	179 probes (160 genes)	320probes (275 genes)
ESFT	113 probes (101 genes)	136probes (124 genes)

Hypermethylation: difference of average β-value >0.3. Hypomethylation: difference of average β-value<−0.3.
doi:10.1371/journal.pone.0062233.t002

Clinical Materials

Clinical specimens from pediatric patients, including 6 each with RTK and Ewing's sarcoma, 21 with CCSK, 9 with CMN, and 41 with Wilms' tumor, used in this study were selected from the files of specimens collected in our laboratory between 1985 and 2001, and the JWiTS (Japan Wilms Tumor Study). In each case, the pathological diagnosis was confirmed by J.H. and H.O. based on morphological observations and the immunophenotypic characteristics. Three non-neoplastic kidney (NK) tissues were obtained from the non-tumorous part of the above specimens.

Sample Preparation

Each disease tissue was evaluated by preparing frozen section and the neoplastic cells accounted for more than 80% of viable

Table 1. Primers used for MassARRAY.

Primer name	5′ - 3′ sequence
ADRA1D_F	aggaagagagTGGTAGGTAATTTGTTTGTTATTTTTTT
ADRA1D_R	cagtaatacgactcactatagggagaaggctCTTCCAACCCAACAAAAACCCTA
ALDOC_F	aggaagagagTTGAATTTGGGTATTTTGAAGATGT
ALDOC_R	cagtaatacgactcactatagggagaaggctCAAATAAAACTACAACCCTAACTCCC
CREG1_F	aggaagagagGTGAGTAATTTGTAGGTGAGTTGGG
CREG1_R	cagtaatacgactcactatagggagaaggctCCACTACACTCCAACCTAAACCA
MGMT_F	aggaagagagTGAGATTGTTAGAGTGTGTTTTTGG
MGMT_R	cagtaatacgactcactatagggagaaggctTCCACTCAAACCAACTAAATTACCTA
PKN1_F	aggaagagagGGTTTTTTTTGGAGAATTAGAAGGG
PKN1_R	cagtaatacgactcactatagggagaaggctCCAACCACCATACAAAAAAATAAAA
PTEN_F	aggaagagagGGGGTTGTAAATAGATTTGATAGGTT
PTEN_R	cagtaatacgactcactatagggagaaggctAAAAAAAATCCCCAAACTAATACCA
THBS1_F	aggaagagagGGAGAGAGGAGTTTAGATTGGTTTT
THBS1_R	cagtaatacgactcactatagggagaaggctACCTTACCCTAAAAAATCCTCCAAC
VHL_F	aggaagagagTTTTGGGGAGATTGATAGATGTAAA
VHL_R	cagtaatacgactcactatagggagaaggctAACCACTTAACCCCAAATAACAAAT

F, forward; R, reverse. Lower case letters indicate tag sequences.
doi:10.1371/journal.pone.0062233.t001

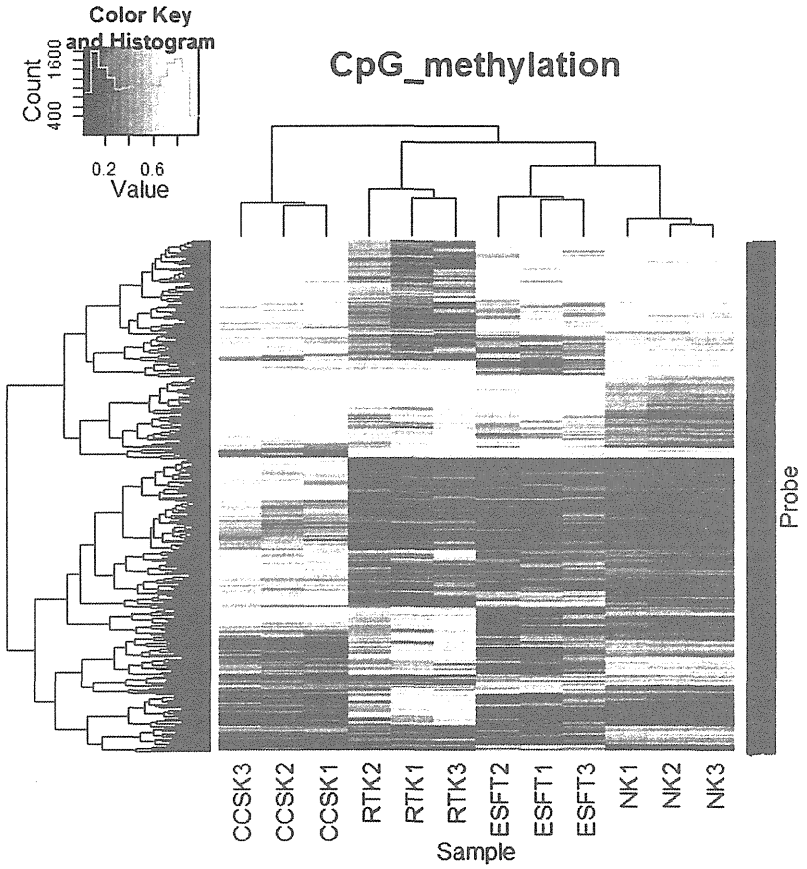

Figure 1. Hierarchical cluster analysis of methylation value (β) in Infinium assay on pediatric tumors. Two-way hierarchical cluster analysis of the methylation level of 1,494 probes (rows, equivalent to hyper- and hypomethylated genes shown in Table 2) and three cases for each of clear cell sarcoma of the kidney (CCSK), rhabdoid tumor of the kidney (RTK), the Ewing's sarcoma family of tumors (ESFT), and non-neoplastic kidney (NK) (columns) were performed using hclust in the R clustering package. The β-values ranged from 0 (unmethylated) to 1 (fully methylated) on a continuous scale.
doi:10.1371/journal.pone.0062233.g001

cells in each sample. The pathologic images of the disease tissues were presented in Figure S1. Genomic DNA was extracted from above evaluated fresh-frozen tissues using the illustra tissue & cells genomicPrep Mini Spin kit (GE Healthcare Bio-Sciences UK Ltd, Chalfont, UK) according to the manufacturer's instructions. The quantity of DNA was assessed by Quant-iT Pico-Green dsDNA Reagent and Kits (Life Technologies Corporation, Carlsbad, CA, USA) and the quality was assessed by agarose gel electrophoresis.

Table 3. The number of specifically methylated genes compared with other each of tumors and non-neoplastic kidney.

	Hypermethylation	Hypomethylation
CCSK	270 genes	28 genes
RTK	65 genes	155 genes
ESFT	7 genes	35 genes

Hypermethylation: difference of average β-value >0.3. Hypomethylation: difference of average β-value<−0.3.
doi:10.1371/journal.pone.0062233.t003

Bisulfite Conversion

Starting from 1 μg of genomic DNA, bisulfite conversion of genomic DNA was performed using the Epitect Bisulfite kit (QIAGEN Inc., Valencia, CA, USA) and EZ DNA Methylation Kit (Zymo Research, Irvine, CA, USA) for the Illumina Infinium Methylation Assay and SEQUENOM MassARRAY, respectively, according to the manufacturer's protocol.

Infinium Methylation Assay

Illumina Infinium HumanMethylation27 (Illumina, Inc., San Diego, CA, USA), containing the 27,578 CpG sites, spanning 14,495 genes, was used for methylation analysis. The bisulfite converted DNA was processed on the chip according to the Illumina protocol. The BeadChips were scanned using iScan system. Our data of Infinium assay have been deposited on Gene Expression Omnibus (GEO) database at the National Center for Biotechnology Information (NCBI, http://www.ncbi.nlm.nih.gov/geo/, series accession number GSE44847). The β-value and the detection p-value for each locus were calculated using GenomeStudio v2010.1. β-value, a ratio of methylated probe signal intensity to sum of methylated and unmethylated probe signal intensities, was used to estimate the methylation

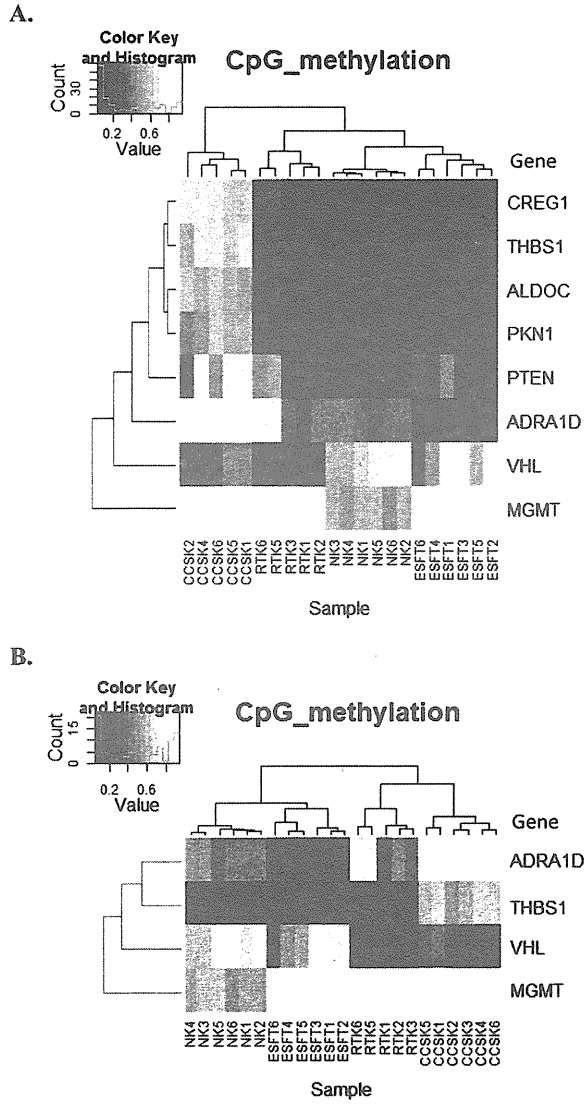

Figure 2. Hierarchical cluster analysis of methylation level of CpG analyzed by MassARRAY. (A) Based on the results indicated in Figure 1, 8 genes were selected as described in the text and analyzed by MassARRAY. Two-way hierarchical cluster analysis was performed using the CpG methylation average of all CpG that have passed QC from each gene. Two cases (RTK4 and CCSK3) showed failed analysis of some CpG sites, and were excluded from hierarchical analysis. (B) Four genes were further selected, and cluster analysis using the methylation average was performed as in (A). CCSK3 was successfully analyzed in all four genes, and included in this analysis.
doi:10.1371/journal.pone.0062233.g002

level of the target locus. Detection p-value is computed from the background model characterizing the chance that the target sequence signal was distinguishable from negative controls. The obtained data were filtered by exclusion of the probes with a detection p-value>0.05 from all probes and SD>0.2 within each entity. The numbers of the detected CpG sites for each sample and filtering process were shown in Table S1. As a result, 23,700 probes (13,385 genes) remained.

EPITYPER Assay (MassARRAY)

The SEQUENOM EpiTYPER assay was performed according to the protocol recommended by the manufacturer. Using the Complete PCR Reagent Set (SEQUENOM Inc., San Diego, CA, USA), target regions were amplified from bisulfite-converted DNAs using the primer pairs containing a T7-promoter tag to allow further *in vitro* transcription. The primers used in this study (Table 1) were designed by EpiDesigner (SEQUENOM). The cycle conditions used were: 95°c for 4 min, 45 cycles of 95°C for 20 s, 56°C (65°C for *CREG1*) for 30 s. and, 95°C for 1 min, and 72°C for 3 min. The PCR products were confirmed by agarose gel electrophoresis. After the dephosphorylation of unincorporated dNTPs by shrimp alkaline phosphatase (SAP) (SEQUENOM), transcription and digestion were performed simultaneously at 37°C for 3 h by RNase A and T7 polymerase (SEQUENOM). The cleavage reactants were purified with CLEAN resin (SEQUENOME) and dispensed onto silicon chips preloaded with matrix (Spectro-CHIPS, SEQUENOM). Mass spectra were collected using a MassARRAY mass spectrometer (Bruker-Sequenom) and analyzed using proprietary peak picking and signal-to-noise calculations (Sequenom Epityper v1.0.5). In MassARRAY analysis, initially, quality control (QC) was performed in each CpG site.

Combined Bisulfite Restriction Analysis (COBRA)

Bisulfite PCR products of *THBS1* produced as described above were digested with the methylation-sensitive restriction enzyme HpyCH4IV (5′-ACGT-3′) (New England Biolabs, NEB, Ipswich, MA, USA) for 12 h at 37°C The digested DNA was separated on 2% agarose gels in 0.5× TBE buffer, stained with ethidium bromide, and visualized on a UV transilluminator. As a control of HpyCH4IV digestion, 0, 50, and 100% methylated DNA were used.

Statistical Analysis

Two-way hierarchical cluster analyses of Infinium assay and MassARRAY were performed using hclust in the R clustering package with Euclidean metric and complete linkage for statistical computing.

Results

DNA methylation profiling of 3 each of CCSK, RTK, ESFT and NK, 12 samples in total, were performed using Infinium HumanMethylation27. First, we analyzed the general methylation status of each tumor group by defining hyper- and hypomethylated CpG sites in each tumor group as those with average β-value differences of >0.3 and <−0.3 compared to NK, respectively. The numbers of selected hyper- and hypomethylated CpG probes in each tumor are listed in Table 2. Among them, the number of selected hypermethylated CpG probes mapped on the CpG island in CCSK, RTK, and ESFT were 490, 130, and 66, respectively, while those of hypomethylated non-CpG probes were 117, 320, and 136, respectively (Table 2).

To test whether the tumors can be distinguished by the methylation level, we performed two-way hierarchical cluster analysis of methylation patterns using hyper- and hypomethylated sites (1,494 probes; equivalent to 1,281 genes selected in Table 2). As shown in Figure 1, each case in the same tumor was clustered in the same group, indicating the tumor-type-dependent methylation pattern of the selected probes.

To further select marker genes for methylation-based tumor-type classification, we defined tumor-specific differentially meth-

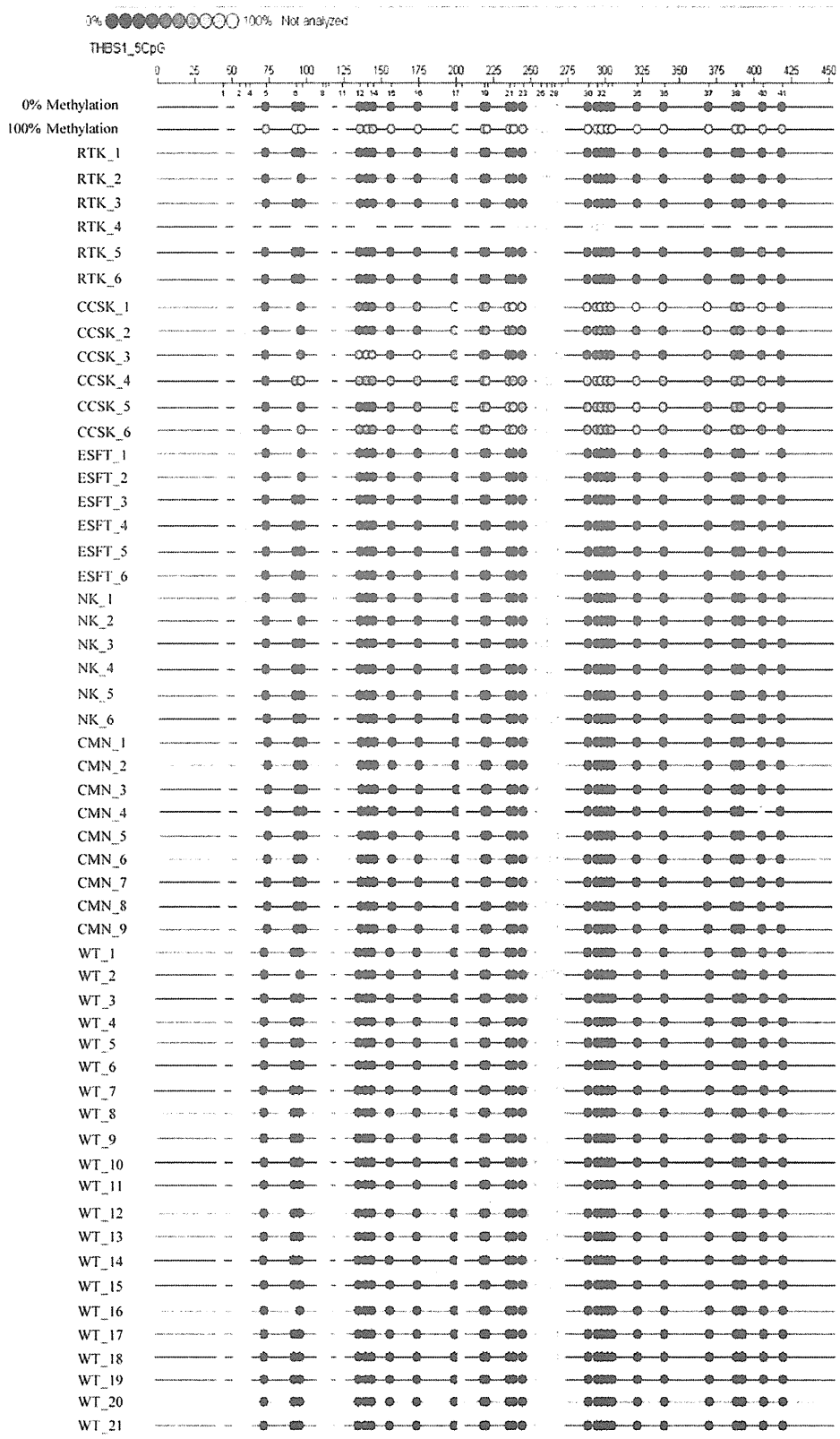
0% 100% Not analyzed
THBS1_5CpG
0% Methylation
100% Methylation
RTK_1
RTK_2
RTK_3
RTK_4
RTK_5
RTK_6
CCSK_1
CCSK_2
CCSK_3
CCSK_4
CCSK_5
CCSK_6
ESFT_1
ESFT_2
ESFT_3
ESFT_4
ESFT_5
ESFT_6
NK_1
NK_2
NK_3
NK_4
NK_5
NK_6
CMN_1
CMN_2
CMN_3
CMN_4
CMN_5
CMN_6
CMN_7
CMN_8
CMN_9
WT_1
WT_2
WT_3
WT_4
WT_5
WT_6
WT_7
WT_8
WT_9
WT_10
WT_11
WT_12
WT_13
WT_14
WT_15
WT_16
WT_17
WT_18
WT_19
WT_20
WT_21

Figure 3. MassARRAY analysis of methylation in *THBS1*. In addition to the 6 cases for each tumor group, 9 and 21 cases of CMN and Wilms' tumor (WT), respectively, were analyzed for DNA methylation of the *THBS1* CpG site, as in Figure 2A. Different colored of circles mark the position of CpG within the sequence (straight line) and the levels of methylation are shown in color (red, low methylation level; yellow, high methylation level). Gray circles represent the unanalyzed CpG sites. WT: Wilms' tumor.
doi:10.1371/journal.pone.0062233.g003

ylated genes as those with average β-value differences of >0.3 (hypermethylated) or <−0.3 (hypomethylated) compared to each of other tumor groups and NK. As shown in Table 3, 270 and 28 genes were identified as CCSK-specific hyper- and hypomethylated genes, respectively, while 65 and 155 genes were selected as RTK-specific hyper- and hypomethylated genes, respectively.

Employing MassARRAY, next we analyzed the surrounding CpG of some specific probes filtered in Table 2, in detail to validate the results of an Infinium assay and further search for candidate genes for a differential diagnostic marker of renal sarcomas. Genes *ALDOC, CREG1, PKN1*, and *Thrombospondin-1 (THBS1)* were selected because of their tendency to be hypermethylated in CCSK by the Infinium assay, while *ADRA1D* was selected because of distinct methylation levels among tumors. *MGMT* and *PTEN* were selected because of hypermethylation in 3 tumors, while *VHL* was selected because of hypomethylation in CCSK and RTK. These are known as tumor suppressor genes and these methylation changes are reportedly involved in specific tumors. [17,18].

We analyzed 6 each of RTK, CCSK, ESFT, and NK, the results of MassARRAY were well correlated with those of the Infinium assay, and each type of tumor revealed a specific DNA methylation pattern (Figure S2). In fact, when we performed two-way hierarchic cluster analysis using the CpG methylation average derived from the results, the cases for each tumor type were successfully classified into the same group (Figure 2A). As shown in Figure 2A, *CREG1, ALDOC, THBS1*, and *PKN1* were hypermethylated in CCSK, whereas RTK, ESFT, and NK were hypomethylated at specific CpG loci, as analyzed by the Infinium assay. *PTEN* was hypomethylated in NK, while variably methylated in sarcoma cases. *ADRA1D* was also hypermethylated in CCSK but hypomethylated in ESFT in comparison with NK, whereas variably methylated in RTK. Although *VHL* was hypomethylated in CCSK and RTK, it was hypermethylated in NK (Figure S3 and Figure S4). *MGMT* was hypermethylated in tumor groups compared to NK.

To distinguish these tumors by the DNA methylation pattern more simply, we further selected four genes characteristically methylated among different tumor groups: *ADRA1D, MGMT, VHL*, and *THBS1*, and performed cluster analysis using the methylation average of 4 genes. As shown in Figure 2B, CCSK, RTK, and ESFT were successfully classified according to the DNA methylation pattern of these genes, suggesting that the DNA methylation analysis of these 4 genes is sufficient for the differential diagnosis of these tumors.

Since *THBS1* was found to be characteristically hypermethylated in CCSK (Figure 2B), we next examined whether the hypermethylation of *THBS1* alone can distinguish CCSK from other tumor groups. To confirm the specificity of *THBS1* hypermethylation in CCSK among pediatric renal tumors, we additionally analyzed Wilms' tumor and CMN. As shown in Figure 3, when we analyzed 6 each of RTK, CCSK, ESFT, and NK as well as 21 cases of Wilms' tumor and 9 cases of CMN, the CpG sites of *THBS1* were unmethylated in all of the cases, indicating that the CpG sites of *THBS1* are specifically hypermethylated in CCSK among pediatric renal tumors.

To detect the methylation of *THBS1* more easily, we have developed combined bisulfite restriction analysis (COBRA) and analyzed 21 cases of CCSK and 41 cases of Wilms' tumor, 6 cases of RTK, 9 cases of CMN, and 6 cases of NK. As shown in Figure 4 and Table 4, the digestion of bisulfite PCR products with HpyCH4IV clearly indicated that a CpG site of *THBS1* in all CCSK cases was hypermethylated. However, none of other tumor groups exhibited hypermethylation of the CpG site of *THBS1*. The results strongly indicate that hypermethylation of *THBS1* is a specific characteristic of CCSK among pediatric renal tumors, and could be utilized as diagnostic maker of this tumor.

Discussion

In this study, we carried out a DNA methylation analysis to identify genes differentially methylated in a series of pediatric tumors and we clearly showed that different pediatric sarcomas occurring in the kidney possess a distinct DNA methylation profile. Especially, CCSK is more frequently hypermethylated, but less hypomethylated, at the CpG island, compared with other tumors. Since pediatric renal sarcomas have overlapping morphologic and clinical features, the significant differences in epigenetic characteristics between these tumors are of particular interest and may represent the distinction of their cell origin or developmental mechanism. We also showed that these tumors can definitely be classified based on the DNA methylation profile, indicating the usefulness of epigenetic profiling for the differential diagnosis of

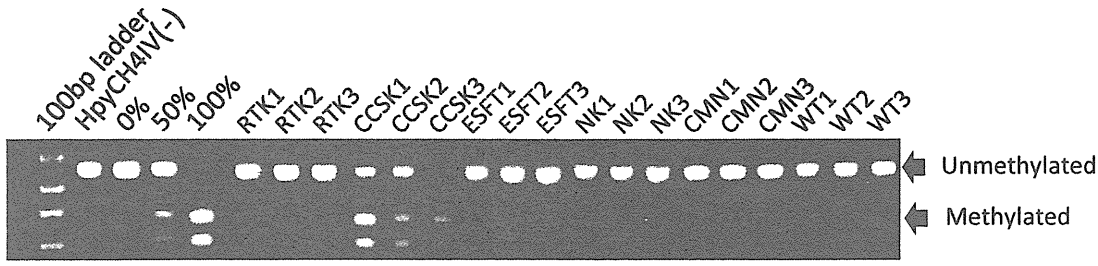

Figure 4. Combined bisulfite restriction analysis (COBRA) of *THBS1* in pediatric renal tumors. Using the same PCR products as in Figure 3, COBRA analysis was performed by digesting with the HpyCH4IV enzyme. The HpyCH4IV site is equivalent to CpG18 (chr15:37,660,642-37,660,645/hg18) in Figure 3. The positions of bands representing methylated and unmethylated DNA are indicated by arrows. As the control of HpyCH4IV digestion, 0, 50, and 100% methylated DNA were loaded on the same gel. WT: Wilms' tumor.
doi:10.1371/journal.pone.0062233.g004

Table 4. Frequency of *THBS1* methylation by COBRA.

	Hypermethylated cases
RTK	0/6
CCSK	21/21
ESFT	0/6
CMN	0/6
Wilms	0/41
NK	0/6

doi:10.1371/journal.pone.0062233.t004

pediatric renal sarcomas, and found that a combination of four genes is sufficient. Furthermore, the DNA methylation status of the *THBS1* CpG site detected by COBRA alone can distinguish CCSK cases from other pediatric renal tumors, including Wilms' tumor and CMN.

The pathological diagnoses of pediatric renal tumors are often supported by immunohistochemical and molecular genetic findings. For example, biallelic inactivation of *SMARCB1* as evidenced by negative immunohistochemical staining has high sensitivity and specificity for the diagnosis of RTK, and *ETV6-NTRK3* fusion is a marker for CMN of the cellular type. In the case of CCSK, however, it has neither immunohistochemical nor molecular genetic markers, while *YWHAE-FAM22* fusion was reported in only a minority [19]. Since *THBS1* hypermethylation is highly specific for CCSK, as we presented in this study, this finding should be useful for a molecular marker of this tumor. Especially, COBRA of the *THBS1* CpG site is highly accurate, reproducible, and can be performed without particular equipment, and, thus, it could be a candidate for routine examination for the differential diagnosis of CCSK from other pediatric renal tumors.

DNA methylation has been proposed as a diagnostic marker for certain cancers. For example, Goto reported that malignant mesothelioma could be differentiated from lung adenocarcinoma by methylation profiles [20], and Mahoney reported that embryonal and alveolar subtypes of rhabdomyosarcoma have a distinct DNA methylation profile [21]. In their cases, however, the methylation status of at least several genes was required for the differentiation of only two entities. In contrast, our findings showed that hypermethylation of a single locus of *THBS1* is sufficient for the differentiation of CCSK from other pediatric tumors and it could serve as a robust diagnostic marker for this tumor.

Hypermethylation of the *THBS1* CpG site has been observed in some tumors. For example, Guo et al. reported that the rate of methylation of *THBS1* was significantly higher in gastric cardia adenocarcinoma than that in the corresponding normal tissues and accompanied by reduction of its mRNA and protein expressions [22], and Guerrero et al. also reported that the hypermethylation of *THBS1* is associated with a poor prognosis in penile squamous cell carcinoma [23]. In both cases, the hypermethylation of *THBS1* has been suggested to be correlated with the pathogenesis.

THBS1 is a member of the thrombospondin family, and is known for putative antiangiogenic factor [24,25]. By employing a knockout mouse model, several studies have shown that the absence of *THBS1* leads to increased vascularization and THBS1 protein inhibits tumor progression in several ways, including direct effects on cellular growth and apoptosis in the stromal compartment [26–29]. Since CCSK is known to be rich in a fine vascular network, it is reasonable to presume that hypermethylation of the *THBS1* CpG site is involved in the pathogenesis of CCSK. However, we observed no significant correlations between the methylation status and expression of THBS1 by realtime RT-PCR and immunohistochemistry (data not shown). This is possibly due to hypermethylated CpG sites of *THBS1* in CCSK that we identified as not being responsible for *THBS1* expression, and other CpG sites are related to the regulation of *THBS1* expression. In fact, other CpG probes (cg19570574: chr15: 37660116–37660117/hg18, cg04051458: chr15: 37660352–37660353/hg18) in the upstream region of the *THBS1* transcription start site were hypomethylated in CCSK based on our assay. Another possibility is that THBS1 is expressed in a limited period during tumorigenesis. Further studies to elucidate the biological significance of CCSK hypermethylation are now underway.

In conclusion, pediatric renal sarcomas possess a distinct DNA methylation profile in a tumor-type-specific manner. The DNA methylation status of the *THBS1* CpG site detected by COBRA alone is sufficient for the distinction of CCSK from other pediatric renal tumors. Although further analysis to elucidate the biological importance of the differential DNA methylation of each tumor is required, our observation should shed light on the significance of the epigenetic diversity of pediatric renal tumors on their biological features and mechanism of pathogenesis.

Supporting Information

Figure S1 Images of frozen tissue sample by H.E. staining. Frozen tumor tissues were embedded in OCT-compound and sectioned in 6 μm, stained with H.E. The proportion of viable tumor tissue was evaluated under light microscope.
(TIF)

Figure S2 Correlation of the methylation values between Infinium assay and MassARRAY. In cases of *THBS1* and *CREG1*, methylation values of same CpG site measured by MassARRAY (average of 6 samples) and Infinium BeadChip Assays (average of 3 samples) were indicated in the scattergrams and values of coefficient of determination (R^2) were calculated. In case of *VHL*, two probe sites were shown. Since each site of *VHL* could not be discriminated from the neighbouring site by MassARRAY, the methylation value was obtained as an average of two sites. Coefficient of determination between the values obtained by two methods was larger than 0.99 in each case. Methylation levels of the equivalent CpG sites were correlated between Infinium assay and MassARRAY.
(TIF)

Figure S3 MassARRAY analysis of *VHL* in pediatric renal tumors. MassARRAY analysis of the *VHL* was carried out in 6 each of RTK, CCSK, ESFT, NK. Different colored of circles mark the position of CpG within the sequence (straight line) and the levels of methylation are shown in color (red, low methylation level; yellow, high methylation level). Gray circles represent the unanalyzed CpG sites. CpG5 and CpG13 are equivalent to Infinium assay probes.
(TIF)

Figure S4 Combined bisulfite restriction analysis (COBRA) of *VHL* in pediatric renal tumors. Bisulfite PCR amplification of *VHL* was carried out by using same primer for MassArray. COBRA analysis was performed by digesting with the TaqI restriction enzyme. The TaqI site is equivalent to CpG3 in MassARRAY analysis. The site of genome sequence is CCGA, which is converted to TaqI sequence (tCGA) by bisulfite reaction. PCR amplification of RTK4 was failed. The digested DNA was

separated on 2% agarose gels in 1×TAE buffer, stained with ethidium bromide, and visualized on a UV transilluminator.
(TIF)

Table S1 Numbers of probes filtered with p-value and SD.
(DOCX)

Acknowledgments

We thank Keiko Nakasato for technical assistance.

References

1. Eble JN, Sauter G, Epstein JI, Sesterhenn IA (2004) World Health Organization Classification of Tumours: Pathology and Genetics of Tumours of the Urinary System and Male Genital Organs. Lyon: IARC Press. p48–61.
2. Rubin BP, Chen CJ, Morgan TW, Xiao S, Grier HE, et al. (1998) Congenital mesoblastic nephroma t(12;15) is associated with ETV6-NTRK3 gene fusion: cytogenetic and molecular relationship to congenital (infantile) fibrosarcoma. Am J Pathol. 153: 1451–1458.
3. Argani P, Perlman EJ, Breslow NE, Browning NG, Green DM, et al. (2000) Clear cell sarcoma of the kidney: a review of 351 cases from the National Wilms Tumor Study Group Pathology Center. Am J Surg Pathol 24: 4–18.
4. Versteege I, Sevenet N, Lange J, Rousseau-Merck MF, Ambros P, et al. (1998) Truncating mutations of hSNF5/INI1 in aggressive pediatric cancer. Nature 394: 203–206.
5. Biegel JA, Tan L, Zhang F, Wainwright L, Russo P, et al. (2002) Alterations of the hSNF5/INI1 gene in central nervous system atypical teratoid/rhabdoid tumors and renal and extrarenal rhabdoid tumors. Clin Cancer Res 8: 3461–3467.
6. Imbalzano AN, Jones SN (2005) Snf5 tumor suppressor couples chromatin remodeling, checkpoint control, and chromosomal stability. Cancer Cell 7: 294–295.
7. Beckwith JB (1994) Renal neoplasms of childhood. 2nd ed. In: Sternberg SS, editor. Diagnostic surgical pathology. New York: Raven Press. 1741–1766.
8. Schuster AE, Schneider DT, Fritsch MK, Grundy P, Perlman EJ (2003) Genetic and genetic expression analyses of clear cell sarcoma of the kidney. Lab Invest 83: 1293–1299.
9. Baylin SB, Belinsky SA, Herman JG (2000) Aberrant methylation of gene promoters in cancer–concepts, misconcepts, and promise. J Natl Cancer Inst 92: 1460–1461.
10. Feinberg AP, Tycko B (2004) The history of cancer epigenetics. Nat Rev Cancer 4: 143–153.
11. Esteller M. (2002) CpG island hypermethylation and tumor suppressor genes: a booming present, a brighter future. Oncogene 21: 5427–5440.
12. Herman JG, Baylin SB (2003) Gene silencing in cancer in association with promoter hypermethylation. N Engl J Med 349: 2042–2054.
13. Anglesio MS, Evdokimova V, Melnyk N, Zhang L, Fernandez CV, et al. (2004) Differential expression of a novel ankyrin containing E3 ubiquitin-protein ligase, Hace1, in sporadic Wilms' tumor versus normal kidney. Hum Mol Genet. 13(18): 2061–2074.
14. Haruta M, Matsumoto Y, Izumi H, Watanabe N, Fukuzawa M, et al. (2008) Combined BuR1 protein down-regulation and RASSF1A hypermethylation in Wilms tumors with diverse cytogenetic change. Mol Carcinog. 47(9): 660–666.
15. Szemes M, Dallosso AR, Melegh Z, Curry T, Li Y, et al. (2013) Control of epigenetic states by WT1 via regulation of de novo DNA methyltransferase 3A. Hum Mol Genet. 22(1): 74–83.
16. Chilukamarri L, Hancock AL, Malik S, Zabkiewicz J, Baker JA, et al. (2007) Hypomethylation and aberrant expression of the glioma pathogenesis-related 1 gene in Wilms tumors. Neoplasia. (11): 970–978.
17. Esteller M, Herman JG (2004) Generating mutations but providing chemosensitivity: the role of O6-methylguanine DNA methyltransferase in human cancer. Oncogene. 23(1): 1–8.
18. Yu J, Ni M, Xu J, Zhang H, Gao B, et al. (2002) Methylation profiling of twenty promoter-CpG islands of genes which may contribute to hepatocellular carcinogenesis. J.BMC Cancer. 2: 29.
19. O'Meara E, Stack D, Lee CH, Garvin AJ, Morris T, et al. (2012) Characterization of the chromosomal translocation t(10;17)(q22;p13) in clear cell sarcoma of kidney. J Pathol. 227(1): 72–80.
20. Goto Y, Shinjo K, Kondo Y, Shen L, Toyota M, et al. (2009) Epigenetic profiles distinguish malignant pleural mesothelioma from lung adenocarcinoma. Cancer Res. 69(23): 9073–9082.
21. Mahoney SE, Yao Z, Keyes CC, Tapscott SJ, Diede SJ (2012) Genome-wide DNA methylation studies suggest distinct DNA methylation patterns in pediatric embryonal and alveolar rhabdomyosarcomas. Epigenetics 7(4): 400–408.
22. Guo W, Dong Z, He M, Guo Y, Guo J, et al. (2010) Aberrant methylation of thrombospondin-1 and its association with reduced expression in gastric cardia adenocarcinoma. J Biomed Biotechnol 721485 Epub 2010 Mar 15.
23. Guerrero D, Guarch R, Ojer A, Casas JM, Ropero S, et al.(2008)Hypermethy-)Hypermethylation of the thrombospondin-1 gene is associated with poor prognosis in penile squamous cell carcinoma. BJU Int. 102: 747–755.
24. Lawler J (2002) Thrombospondin-1 as an endogenous inhibitor of angiogenesis and tumor growth. J Cell Mol Med 6: 1–12.
25. Folkman J (2004) Endogenous angiogenesis inhibitors. APMIS 112: 496–507.
26. Greenaway J, Lawler J, Moorehead R, Bornstein P, Lamarre J, et al.(2007) Thrombospondin-1 inhibits VEGF levels in the ovary directly by binding and internalization via the low density lipoprotein receptor-related protein-1 (LRP-1). J Cell Physiol 210: 807–818.
27. Wang S, Wu Z, Sorenson CM, Lawler J, Sheibani N (2003) Thrombospondin-1-deficient mice exhibit increased vascular density during retinal vascular development and are less sensitive to hyperoxia-mediated vessel obliteration. Dev Dyn 228: 630–642.
28. Lawler J, Miao WM, Duquette M, Bouck N, Bronson RT, et al. (2001) Thrombospondin-1 gene expression affects survival and tumor spectrum of p53-deficient mice. Am J Pathol 159: 1949–1956.
29. Sund M, Hamano Y, Sugimoto H, Sudhakar A, Soubasakos M, et al. (2005) Function of endogenous inhibitors of angiogenesis as endothelium-specific tumor suppressors. Proc Natl Acad Sci USA 102: 2934–2939.

Author Contributions

Conceived and designed the experiments: HU HO NK. Performed the experiments: HU HO SA KN. Analyzed the data: HU HO. Contributed reagents/materials/analysis tools: HO JF JH MF KN KH. Wrote the paper: HU HO KK NK.